RSC Advances

PAPER

View Article Online
View Journal | View Issue

Cite this: *RSC Adv.*, 2017, **7**, 48184

Wettability of monolayer graphene/single-walled carbon nanotube hybrid films

Xiannian Chi,[ab] Jian Zhang,[ab] Jean Pierre Nshimiyimana,[ab] Xiao Hu,[ab] Pei Wu,[ab] Siyu Liu,[a] Jia Liu,[ab] Weiguo Chu*[a] and Lianfeng Sun*[a]

Received 7th September 2017
Accepted 3rd October 2017

DOI: 10.1039/c7ra09934g

rsc.li/rsc-advances

The wettability of monolayer graphene has been reported to be transparent. In this work, we study the wettability of monolayer graphene using single-walled carbon nanotube (SWNT) films as the substrate. Compared to the water contact angles of 86.3° for monolayer graphene and 131.6° for SWNTs, the water contact angle of the graphene/SWNT hybrid films is found to be 106.5°. This suggests that the wettability of monolayer graphene is not transparent, but somewhat half-transparent. The mechanisms of these results are suggested and discussed. Considering the atomic thickness of graphene materials, the modification of the wettability of surfaces by applying graphene materials on the underlying substrates provides wide potential applications for wettability control.

Introduction

The surface of a material is the most important part determining the compatibility with its environment.[1] The wettability, which has been researched in many fields recently,[2–4] is one of the most important characteristics of a solid interface.[5] It can reflect changes in the characteristics of a solid surface, including the chemical composition and the geometric structure.[6] Furthermore, the wettability has a broad influence on the applications of materials for various industries,[7] such as the biomedical, automobile and paint industries. In many cases, although the bulk properties are excellent for a specific application, the surface may need to be modified and engineered in the desired direction.[8] This is especially important for materials used in hybrid materials, coatings, and biological media,[9] because the surface charge, hydrophilicity, and wettability are important.[10–12]

The water wettability of graphene (Gr) has been shown to affect the energy storage capacity of a graphene supercapacitor[13] and the heat exchange between a graphene-coated copper substrate and water vapour.[14] Despite the fact that vast research efforts have revealed a great deal of the unique electronic,[15] optical and mechanical properties of graphene,[16] a simple yet unanswered question is whether atoms or molecules located on one side of the lattice experience electrostatic or van der Waals interactions exerted by atoms or molecules on the other side.[12,17,18] Carbon nanotubes (CNTs) are of tremendous interest for both fundamental and applied research since they show unique properties.[19] Recently, the wettability of SWNT surfaces has been a subject of extensive investigation because of their potential applications.[19–21] Due to the special nanostructures and surface properties of CNTs, further surface functionalization or textured arrangements could facilitate easy control of their wetting properties. Therefore, it is fundamentally important and practically critical to understand and control the water wettability of CNT hybrid materials.[22] In spite of intense activity in carbon nanotube research, there are very few reports studying water–CNT–graphene interactions, which could be important if graphene is to be used in conformal coatings.

Motivated by this, we performed water contact-angle measurements on monolayer graphene/single-walled carbon nanotube hybrid films. Research on the wetting properties of graphene has been used as a first step towards quantifying its role in the transmission of such interactions, as the interfacial energies involved directly determine the macroscopic contact angle, θ, of a liquid droplet on a hybrid film.

Experimental

The SWNT films were fabricated by floating catalytic chemical vapor deposition (FCCVD). As a catalyst source, ferrocene/sulfur powder is heated to 65–75 °C and flowed into the reaction zone by a mixture of 1000 sccm argon and 1–10 sccm methane. The temperature of the catalyst and the flow of methane can be tuned to produce different samples. The quality of the SWNTs was studied by Raman spectroscopy and scanning electron microscopy (SEM). The micro-Raman measurements were performed with a Renishaw inVia Raman Spectroscope under ambient conditions with laser excitation at 514.5 nm (2.41 eV) induced by an argon ion laser. The laser power is controlled at 1 mW and the spatial resolution of the laser spot is ~1 μm. The

[a]*CAS Key Laboratory of Nanosystem and Hierarchical Fabrication, CAS Center for Excellence in Nanoscience, National Centre for Nanoscience and Technology, Beijing 100190, China. E-mail: slf@nanoctr.cn; wgchu@nanoctr.cn*

[b]*University of Chinese Academy of Sciences, Beijing 100049, China*

SEM measurements were taken under high vacuum (103 Pa or lower) and the accelerating voltage is set at 10 kV using a Hitachi S-4800 field-emission system. For the pristine SWNT film samples, the SWNTs were immersed in deionized water to cause them to adhere tightly to the silicon wafer, followed by air drying. Since the structure of pristine SWNTs is very fluffy, we condensed the SWNT bundles by dropping ethanol onto the films, and then the films were dried in air. Large-area monolayer graphene films were synthesized by chemical vapour deposition (CVD) on Cu foils using methane as the precursor at 1030 °C.

Results and discussion

By adjusting the parameters of the FCCVD system, such as the catalyst sublimation temperature and the deposition duration, to the optimized ones, we have obtained high quality SWNT films. After transferring the SWNT films onto silicon wafers, we dropped ethanol onto them in order to condense the SWNTs.

Large-area monolayer graphene films were synthesized by chemical vapour deposition (CVD) on Cu foils using the liquid precursor hexane. After growth, a thin poly(methyl methacrylate) (PMMA) film was coated onto the graphene/Cu substrate. The underlying Cu substrate was dissolved in dilute HNO_3, and the film was transferred onto the substrates.[23] Fig. 1(a) shows a schematic diagram of the fabrication process of the hybrid film. Firstly, we transferred the SWNT film onto a silicon wafer, and then after putting PMMA/graphene onto it, we dried it at 70 °C in air for 10 minutes. Next, we immersed the film in acetone to etch the PMMA. Finally, we obtained a hybrid film. Fig. 1(b) shows an optical image of a hybrid film before etching the PMMA (step (5)). The areas with different colours correspond to different films as marked. The boundaries between films can be clearly observed. Fig. 1(c) shows an optical image of the hybrid film after etching the PMMA (step (6)). It can be clearly seen that after PMMA etching, the films are much more uniform, indicating the high quality of the films.

Fig. 2(a) shows a typical SEM image of the SWNT films on the silicon wafers. Raman spectroscopy, known as a convenient and non-destructive technique, is widely used in probing the microstructures of carbon materials. In order to confirm the characteristics of the SWNT films, we recorded the Raman spectra of the SWNT films. Fig. 2(b) shows a typical Raman spectrum of a SWNT film. It can be seen that the SWNTs are in the form of bundles, which are curled and randomly oriented. We can see that the D peak of the SWNT films can almost be ignored, which proves that the SWNT films are of high quality.[24] To research the wetting properties of the SWNT films, we measured the contact angles (CAs) of deionized water droplets (1 mL) on the SWNT films (OCA20 CA, Dataphysics), as shown in the inset of Fig. 2(a) where the CA is 131.6°.

It should be noted that the SWNTs used in this work were not purified, and contain some amount of iron catalysts. We have checked the distribution of these catalysts with TEM. As shown in Fig. 3, the catalysts are usually nanoparticles with sizes of about 3 nm, which are embedded in the SWNT bundles. The SWNTs used in this work are in the form of bundles with diameters in the range of 30–50 nm, which are curled and randomly oriented. Therefore, these catalysts are believed to have no effect on the contact angles of the SWNTs and the hybrid film.

For characterization purposes, a graphene film was transferred to a silicon wafer using poly(methyl methacrylate) as the transferring agent. It is widely accepted that the contact angle of graphene highly depends on the amount and kind of contaminants. In this work, the main organic compound that may contaminate the surface of graphene is PMMA. Therefore, the following treatments are used before measuring the contact angle of the hybrid films: the film was immersed into acetone

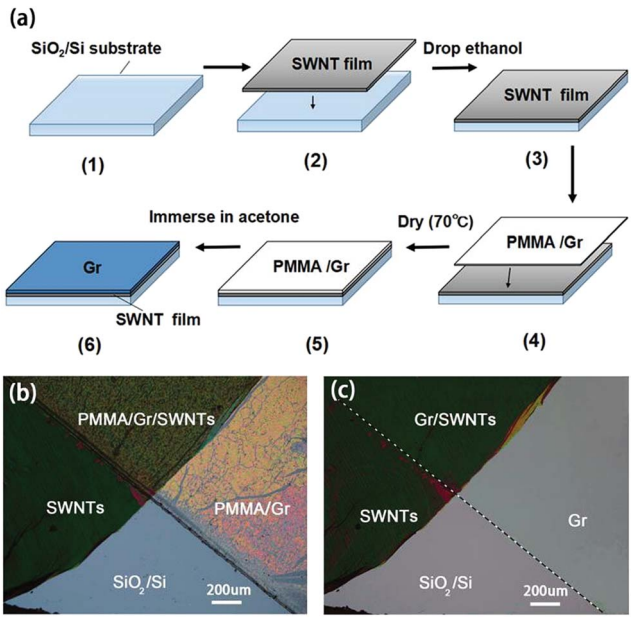

Fig. 1 (a) Schematic diagram showing the fabrication process of the hybrid film of graphene on SWNTs. (b) A typical optical image of the PMMA/Gr/SWNTs, SWNTs, PMMA/Gr, and SiO_2/Si before removing the PMMA, which corresponds to step (5) in (a). The areas with different colours correspond to different films as marked. The boundaries between films can be observed clearly. (c) An optical image of the same area of (b) after removing the PMMA (step (6)). The uniform colours of the graphene and Gr/SWNT films suggest high quality.

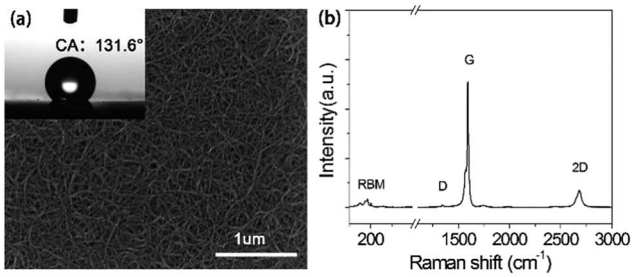

Fig. 2 (a) A typical SEM image of a SWNT film. It can be seen that the SWNTs are in the form of bundles with diameters in the range of 30–50 nm, which are curled and randomly oriented. The inset shows an optical image of a water droplet placed onto the surface of a SWNT film. The water contact angle (CA) is 131.6°, indicating hydrophobic properties. The average contact angle over 60 pristine SWNT films is 130.6°. (b) Typical Raman spectrum of a SWNT film.

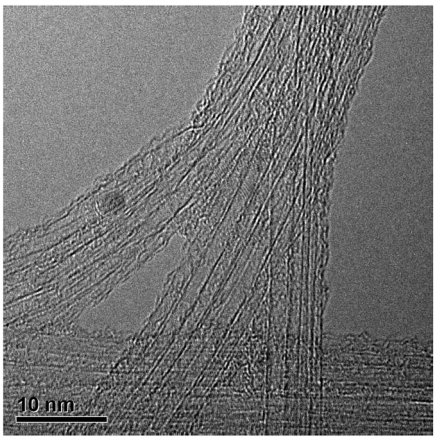

Fig. 3 TEM image of SWNTs. The catalysts are usually nanoparticles with sizes of about 3 nm, which are embedded in the SWNT bundles.

for about 10 minutes, which was followed by an IPA rinse. During this process, the PMMA on the graphene surface can be dissolved. After this, the hybrid film was heated to ~375 °C in a furnace with constant argon–hydrogen flow and this temperature was held for ~1 h. The trace PMMA remaining on the graphene surface was evaporated. This technique for cleaning graphene has been reported previously.[18]

Shown in Fig. 4(a) is a micro-Raman spectrum of a graphene sample after transfer to a silicon wafer. The Raman spectrum of graphene is dominated by two prominent features: the G band and the 2D band. By combining the intensities of the G and 2D bands, one can reliably estimate the number of graphene layers. The ratio of the 2D peak intensity to G peak intensity (I_{2D}/I_G) is 3.2. A clear shift in the position of the 2D peak is observed (Fig. 4(b)), and it is at 2686 cm^{-1}. This result is consistent with the literature;[18] Ferrari *et al.* have reported that, as the number of layers in graphene films is reduced, the 2D peak shifts towards the lower frequency range, and for single-layer graphene it appears between 2650 and 2700 cm^{-1}. Also, as reported for the case of water on supported graphene, about 30% of the van der Waals interactions between the water and the substrate are transmitted through the one-atom-thick layer.[18] We tested

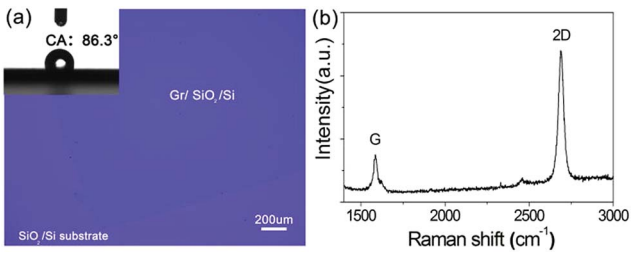

Fig. 4 (a) Optical image of a monolayer graphene film on a SiO_2/Si substrate. The inset shows an optical image of a water droplet placed onto the surface of the monolayer graphene. The water contact angle is 86.3°, indicating hydrophilic properties. (b) Typical Raman spectrum of graphene on a SiO_2/Si substrate. The ratio of the 2D peak intensity to the G peak intensity (I_{2D}/I_G) is 3.2, indicating that the graphene is a monolayer.

the CAs of water droplets on the graphene films; the result (86.3°) is similar to other reports,[25] and the inset of Fig. 4(a) shows an optical image of a water droplet placed onto the surface of monolayer graphene. The dark blue part is the monolayer graphene on the substrate.

The interaction between graphene and SWNTs is attributed to be van der Waals forces due to the following fabrication processes: the hybrid film was immersed in acetone for about 10 minutes, which was followed by an IPA rinse. During this process, the PMMA on the graphene surface can be dissolved. After this, the hybrid film was heated to ~375 °C in a furnace with constant argon–hydrogen flow and this temperature was held for ~1 h.

Except for the influence of the net electric field at the substrate–droplet interfaces, the wettability of a solid surface, is also strongly influenced both by its chemical composition and by its geometric structure (or surface roughness). If the films are sufficiently rough, the liquid may trap air, which could induce a composite surface effect. In this case, the relationship between the CA of the flat surface θ and that of the suitably rough surface is expressed by the Cassie and Baxter equation:[26]

$$\cos\theta_r = rf_1\cos\theta - f_2, \quad (1)$$

where r is the roughness factor (which is defined as the ratio of the actual surface area of a rough surface to the projected area), and f_1 and f_2 are the fractions of the nanotubes and air on the SWNT films, respectively. The Cassie and Baxter equation indicates that the CA θ_r increases with an increasing fraction of air (f_2). However, the as-grown SWNT films were also condensed when they were immersed in water. In order to eliminate the influence of water when the SWNT films are rinsed and confirm that the decrease in the CAs of the water droplets on the hybrid films is not introduced by the water, we dropped ethanol onto the SWNT films before coating them with graphene. As the experiments show, the SWNT bundles are much tighter just like the films which are picked out from water, and the CAs of water droplets on these two kinds of condensed SWNT films exhibit no differences.

When the SWNT films were dry, we first tested the static CA of a water droplet on them and then made some hybrid films. Using PMMA as the transferring agent, graphene was transferred to a silicon wafer whose surface already contained SWNT films. The hybrid film was then obtained. After the hybrid films were dried in ultra-clean chamber, we tested again the CAs of water droplets on the surface of the samples. For statistics, 6–10 separate measurements were performed at different locations on the sample surface and the results were averaged to obtain the mean and standard deviation. The average contact angle (CA) of water droplets on the hybrid films is 106.5°, which is different from that on pristine SWNT films (130.6°) and graphene (86.3°).

As shown in Fig. 5(a), the CAs decreased obviously after the SWNT films were coated with graphene. Compared with the SWNT films, the CAs of water droplets on the hybrid films are smaller.

On the basis of Young's equation,[27] the contact angle can be given as follows:

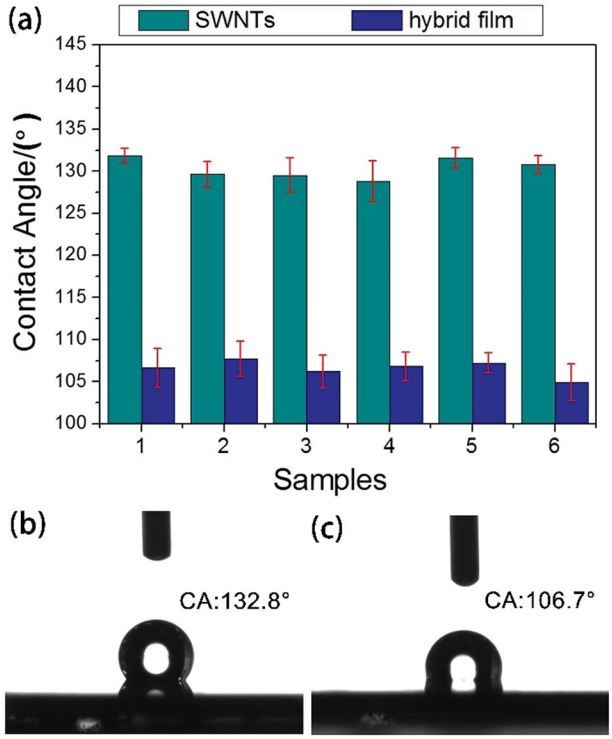

Fig. 5 (a) Comparison of the water contact angles of 6 SWNT films and 6 hybrid films. The average contact angle over 100 measurements of water droplets on the hybrid films is 106.5°. This suggests that the wettability of monolayer graphene is not transparent, but somewhat half-transparent. (b) Typical optical images of a water droplet placed onto the surface of SWNTs. The water contact angle (CA) is 132.8°. (c) Typical optical image of a water droplet placed onto the surface of a hybrid film. The water contact angle (CA) is 106.7°, indicating hydrophobic properties.

$$\gamma_s = \gamma_{sl} + \gamma_l \cos\theta, \quad (2)$$

where γ_s, γ_l, and γ_{sl} represent the solid surface free energy, liquid surface free energy, and solid–liquid interfacial energy, respectively. θ is the contact angle between the solid surface and the liquid. On the other hand, the work of adhesion (W_{sl}) between a solid surface and a liquid can be described by eqn (3):

$$W_{sl} = \gamma_s + \gamma_l - \gamma_{sl}. \quad (3)$$

Combining eqn (2) and (3) results in eqn (4):

$$W_{sl} = \gamma_l(1 + \cos\theta). \quad (4)$$

According to eqn (4), the W_{sl} (SWNT films), W_{sl} (graphene), and W_{sl} (hybrid films) are $0.25\gamma_l$, $1.06\gamma_l$, and $0.71\gamma_l$, respectively. It is obvious that W_{sl} (graphene) is much higher than W_{sl} (SWNT films). Therefore, when the SWNT film surface is covered with graphene, the work of adhesion between the hybrid films and water will increase compared with SWNT films, and the CAs of water droplets on the hybrid films will decrease correspondingly.

It is well known that wettability is decided simultaneously by chemical composition and the geometrical microstructure of the surface. As graphene is a famous material with a zero electronic band gap, such charge induction may affect the electronic structure of the contacting graphene. Graphene coatings do not significantly disrupt the intrinsic wetting behaviour of surfaces for which surface–water interactions are dominated by van der Waals forces. On the surface of SWNTs, where van der Waals forces control the wetting, we find that graphene remains half-transparent to the substrate wetting behaviour and remains non-invasive to the substrate/water interface. Another issue worth noting is that most SWNTs exist in the form of bundles in the SWNT films and the arrangement of the SWNT bundles is completely random. Hence, the roughness of the hybrid films is much higher than that of graphene films. According to eqn (1) and (4), the CAs of water droplets on the hybrid films should be bigger than those on graphene and smaller than those on SWNT films, which is consistent with our CA measurements.

Conclusions

In summary, we have fabricated SWNT films and graphene successfully. We also investigated the wettability of the pristine materials and their hybrid films. As far as we know, this is the first time that the wettability of these hybrid films has been researched using the above method. We found that the wettability of the hybrid films changed, which can be demonstrated by the contact angle decreasing. This result suggests that the wettability of monolayer graphene is not transparent, but somewhat half-transparent. Compared with other methods, this can keep the unique properties of the SWNT films without damaging the structure of the bottom part of the SWNT films. This study exemplifies the synergistic integration between the 2D graphene and 1D SWNTs for novel applications. Furthermore, the demonstrated 2D carbon will also warrant other novel applications. We believe that the manipulation of the wetting properties of these hybrid films will be greatly facilitated by fundamental principles and theoretical studies. Combining the properties of hybrid films, we believe that these kinds of hybrid films have greater application potential.

Conflicts of interest

There are no conflicts to declare.

Acknowledgements

This work was supported by the National Science Foundation of China (Grant No. 51472057) and the Major Nanoprojects of Ministry of Science and Technology of China (2016YFA0200403). W. G. C. acknowledges financial support from the Strategic Priority Research Program of the Chinese Academy of Sciences (Grant XDA09040101).

Notes and references

1 S. Wang, Y. Zhang, N. Abidi and L. Cabrales, *Langmuir*, 2009, **25**, 11078–11081.
2 X. Gao and L. Jiang, *Nature*, 2004, **432**, 36.
3 F. Guo and Z. Guo, *RSC Adv.*, 2016, **6**, 36623–36641.

4 S. Nagappan, S. S. Park and C. S. Ha, *J. Nanosci. Nanotechnol.*, 2014, **14**, 1441–1462.
5 H. Y. Erbil, A. L. Demirel, Y. Avci and O. Mert, *Science*, 2003, **299**, 1377–1380.
6 J. Zhang, H. Feng, W. Zao, M. Ling and Y. Zhao, *RSC Adv.*, 2014, **4**, 48443–48448.
7 Y. Liu, J. Chen, D. Guo, M. Cao and L. Jiang, *ACS Appl. Mater. Interfaces*, 2015, **7**, 13645–13652.
8 C. Hao, *et al.*, *Nat. Commun.*, 2015, **6**, 7986.
9 P. Tao, W. Shang, C. Song, Q. Shen, F. Zhang, Z. Luo, N. Yi, D. Zhang and T. Deng, *Adv. Mater.*, 2015, **27**, 428–463.
10 A. I. Aria and M. Gharib, *Langmuir*, 2014, **30**, 6780–6790.
11 D. W. Jeong, U. H. Shin, J. H. Kim, S. H. Kim, H. W. Lee and J. M. Kim, *Carbon*, 2014, **79**, 442–449.
12 J. Rafiee, M. A. Rafiee, Z. Z. Yu and N. Koratkar, *Adv. Mater.*, 2010, **22**, 2151–2154.
13 J. R. Miller, R. A. Outlaw and B. C. Holloway, *Science*, 2010, **329**, 1637–1639.
14 M. Ma, G. Tocci, A. Michaelides and G. Aeppli, *Nat. Mater.*, 2015, **15**, 66.
15 X. Chi, L. Chang, D. Xie, J. Zhang and G. Du, *Mater. Lett.*, 2013, **106**, 178–181.
16 S. W. Lee, S. J. Park, E. E. B. Campbell and Y. W. Park, *Nat. Commun.*, 2011, **2**, 220.
17 Z. Li, *et al.*, *Nat. Mater.*, 2013, **12**, 925–931.
18 J. Rafiee, X. Mi, H. Gullapalli, A. V. Thomas, F. Yavari, Y. Shi, P. M. Ajayan and N. A. Koratkar, *Nat. Mater.*, 2012, **11**, 217–222.
19 Y. Homma, S. Chiashi, T. Yamamoto, K. Kono, D. Matsumoto, J. Shitaba and S. Sato, *Phys. Rev. Lett.*, 2013, **110**, 157402.
20 A. H. Barber, S. R. Cohen and H. D. Wagner, *Phys. Rev. Lett.*, 2004, **92**, 186103.
21 Z. Xu, L. Chen, B. Zhou, Y. Li, B. Li, J. Niu, M. Shan, Q. Guo, Z. Wang and X. Qian, *RSC Adv.*, 2013, **3**, 10579.
22 S. Wang, H. Liu, D. Liu, X. Ma, X. Fang and L. Jiang, *Angew. Chem., Int. Ed.*, 2007, **46**, 3915–3917.
23 A. Srivastava, *et al.*, *Chem. Mater.*, 2010, **22**, 3457–3461.
24 M. S. Dresselhaus, A. Jorio, M. Hofmann, G. Dresselhaus and R. Saito, *Nano Lett.*, 2010, **10**, 751–758.
25 R. Raj, S. C. Maroo and E. N. Wang, *Nano Lett.*, 2013, **13**, 1509–1515.
26 C. J. Shih, M. S. Strano and D. Blankschtein, *Nat. Mater.*, 2013, **12**, 866–869.
27 X. M. Li, D. Reinhoudt and M. Crego-Calama, *Chem. Soc. Rev.*, 2007, **36**, 1350–1368.